Inorganic Chemistry

pubs.acs.org/IC Article

Prediction and Synthesis of Dysprosium Hydride Phases at High Pressure

Nilesh P. Salke, M. Mahdi Davari Esfahani, N. Yedukondalu, Youjun Zhang, Ivan A. Kruglov, Jianshi Zhou, Eran Greenberg, Vitali B. Prakapenka, Jin Liu,* Artem R. Oganov,* and Jung-Fu Lin*

Cite This: https://dx.doi.org/10.1021/acs.inorgchem.9b03078 Read Online

ABSTRACT: Crystal structure prediction (CSP) methods recently proposed a series of new rare-earth (RE) hydrides at high pressures with novel crystal structures, unusual stoichiometries, and intriguing features such as high-T_c superconductivity. RE trihydrides (REH_3) generally undergo a phase transition from ambient $P6_3/mmc$ or $P\bar{3}c1$ to $Fm\bar{3}m$ at high pressure. This cubic REH_3 ($Fm\bar{3}m$) was considered to be a precursor to further synthesize RE polyhydrides such as YH_4, YH_6, YH_9, and CeH_9 with higher hydrogen contents at higher pressures. However, the structural stability and equation of state (EOS) of any of the REH_3 have not been fully investigated at sufficiently high pressures. This work presents high-pressure X-ray diffraction (XRD) measurements in a laser-heated diamond anvil cell up to 100 GPa and ab initio evolutionary CSP of stable phases of DyH_3 up to 220 GPa. Experiments observed the $Fm\bar{3}m$ phase of DyH_3 to be stable at pressures from 17 to 100 GPa and temperatures up to ~2000 K. After complete decompression, the $P\bar{3}c1$ and $Fm\bar{3}m$ phases of DyH_3 recovered under ambient conditions. Our calculations predicted a series of phases for DyH_3 at high pressures with the structural phase transition sequence $P\bar{3}c1 \rightarrow Imm2 \rightarrow Fm\bar{3}m \rightarrow Pnma \rightarrow P6_3/mmc$ at 11, 35, 135, and 194 GPa, respectively. The predicted $P\bar{3}c1$ and $Fm\bar{3}m$ phases are consistent with experimental observations. Furthermore, electronic band structure calculations were carried out for the predicted phases of DyH_3, including the *4f* states, within the DFT+U approach. The inclusion of *4f* states shows significant changes in electronic properties, as more Dy *d* states cross the Fermi level and overlap with H *1s* states. The structural phase transition from $P\bar{3}c1$ to $Fm\bar{3}m$ observed in DyH_3 is systematically compared with other REH_3 compounds at high pressures. The phase transition pressure in REH_3 shows an inverse relation with the ionic radius of RE atoms.

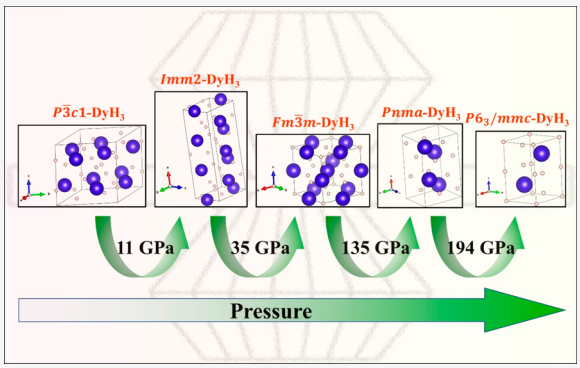

INTRODUCTION

Metal hydride formation has been of huge scientific interest, as hydrides are known for their unique optical and superconducting properties as well as for potential hydrogen storage applications.[1−3] Hydrogen reacts with most metals to form an interstitial hydrides with variable hydrogen concentrations.[4] Among them, rare-earth hydrides (REH_x) have been of particular research interest lately, as RE atoms possess partially filled *f* orbitals[5] while hydrogen with one electron can accept or donate one electron or form covalent bonds.[6] Several experimental works have been recently carried out on RE hydrides due to the interesting electronic states predicted.[7−13] Under ambient conditions, RE elements react with hydrogen to form dihydrides, REH_2, with metallic conductivity. Further absorption of hydrogen results in the formation of RE trihydrides (REH_3), with an electrically insulating character. These lead to the possibility of engineering the composition-dependent switching of electrical and optical properties in REH_x.[1]

Applied pressure on RE with hydrogen can provide a tremendous amount of internal energy and induce metallization, electronic, magnetic, and structural transitions, exotic physical properties, or formation of new compounds with unusual stoichiometries. REH_3 species are known for their interesting high-pressure behavior.[7−9,14−16] In this respect, many REH_3 species (RE = Sc, Y, Sm, Gd, Tb, Ho, Er, Lu, Dy) have been studied experimentally[7,8,14−16] and theoretically[9] under pressure. However, most of these studies are limited to ~35 GPa or below. Under ambient conditions, REH_3 species generally crystallize into a $P6_3/mmc$ or $P\bar{3}c1$ structure.[9] With further pressurization, they undergo a structural transition into a $Fm\bar{3}m$ structure via an intermediate mixed phase or complex

Received: October 21, 2019

phase region.[7,8,14−16] The high-pressure phase transition sequence, from $P6_3/mmc$ or $P\bar{3}c1$ to $Fm\bar{3}m$, appears to be prevalent in REH_3 systems.[7,8,14−16] Theoretical investigations of REH_3 compounds have focused on their structural stability, phase transitions, equation of state (EOS), electronic/electrical and phonon properties.[9] For some studies at pressures above 35 GPa, REH_3 species have been reported to be the precursor phase for RE hydrides with higher hydrogen contents.[13,17−19] Hence, the high pressure−temperature ($P-T$) phase stability and physical properties of the $Fm\bar{3}m$ phase above 35 GPa have greatly inspired our recent pursuit of RE polyhydrides with high hydrogen contents and/or superconductivity at high pressures.

Crystal structure prediction (CSP) has become a powerful research tool to predict materials at ambient as well as at high pressure.[10,11] Many hydrogen-rich RE polyhydrides/superhydrides have been predicted to become stable under pressure.[10,17,20] Those hydrides have hydrogen contents greater than what would follow from atomic valencies. Experimentally the concentration of hydrogen can be implied through the expansion of the unit cell volume with changes in the bonding nature between the RE atom and hydrogen. The hydrogen content also has a significant effect on the structural, electronic, and magnetic properties of RE hydrides. RE hydrides are also very interesting systems to investigate theoretically, as a variety of electronic states are expected to change at high pressure. Many of them are expected to exhibit superconductivity close to room temperature.[10,17,18,20] Extensive efforts are taken by theorists and experimentalists to discover hydride-based superconductors.[10,17,18,20−22] Superconductivity is governed by the interactions between hydrogen and metal atoms in certain crystal structures, which can be seen from the very distinct T_c values for various hydrides of different RE atoms.[10,11,13,17,20] RE superhydrides (REH_x, $x > 5$) with stoichiometries REH_6, REH_9, and REH_{10} are predicted to form novel clathrate structures. These clathrate-structured RE superhydrides possess a three-dimensional dense hydrogen sublattice which encapsulates RE atoms.[10,17,20] Interestingly, these superconducting RE superhydrides were predicted to crystallize in highly symmetric crystal structures at high pressures. For example, YH_6 is predicted to crystallize in the cubic $Im\bar{3}m$ structure,[17] YH_{10} and LaH_{10} are predicted to crystallize in the cubic $Fm\bar{3}m$ structure,[10,20] and YH_9 and CeH_9 predicted to have a hexagonal $P6_3/mmc$ structure.[10,13] Experimentally synthesized and characterized YH_6, YH_9, CeH_9, PrH_9, and LaH_{10} were consistent with their theoretically predicted structures and high-pressure phase stability.[13,18,19,23,24] Most of these clathrate-structured RE superhydrides were predicted to have a superconducting T_c value close to room temperature.[10,17,19,20] Notably, following recent theoretical predictions, high-temperature superconductivity was experimentally observed in LaH_{10} with a record high T_c of 250 K at 170 GPa.[18]

The high-pressure $Fm\bar{3}m$ phase of YH_3 was also predicted to be a conventional superconductor under pressure.[25] In recent studies on the Ce−H system, CeH_3 with a β-UH_3 type structure (space group $Pm\bar{3}n$, β-CeH_3) was synthesized at 33 GPa after laser heating.[13] After further compression and reheating of β-CeH_3 and H_2, CeH_9 was formed at pressures of 80−100 GPa.[13] In the Pr−H system, PrH_3 phases with $Fm\bar{3}m$ and $P4/nmm$ structures were synthesized at 10 and 40 GPa, respectively.[24] The point to be noted here is that the Ce−H and Pr−H systems were studied in the environment with excess hydrogen.[13,24] Studies on RE in excess hydrogen under a megabar pressure regime and with laser heating resulted in discoveries of β-UH_3-type CeH_3, $P4/nmm$-PrH_3, LaH_{10}, CeH_9, and PrH_9 phases.[12,13,24] However, the RE−H binary systems that produced new RE hydrides with stoichiometries and structures were light lanthanoids. Importantly, they have been investigated at pressures over the megabar range. For other RE elements, particularly heavy lanthanoids such as Dy, Ho, and Er, their possible hydride phases have not been explored experimentally at megabar pressures, at high-temperatures and in excess of hydrogen. In a recent report, heavy lanthanoids were reported to possibly be low T_c superconductors.[11]

Dysprosium (Dy), one of the heavy, normally trivalent lanthanoids, is known to form di- and trihydrides under ambient conditions.[16,26] High-pressure X-ray diffraction (XRD) studies on DyH_3 reported up to 35 GPa found the HCP to FCC transition, as for other REH_3 compounds.[16] Recently, Peng et al.[10] and Semenok et al.[11] predicted rich chemistry of the Dy−H system e.g., DyH, DyH_2, DyH_3, DyH_4, DyH_6, DyH_7, Dy_5H_{14}, and DyH_9. It would be interesting to investigate Dy−H chemistry under extreme conditions.[10,11] The structural stability of the $Fm\bar{3}m$ phase of DyH_3 under high $P-T$ conditions has not been studied; hence, its experimental and theoretical investigations would be very intriguing.

Here we conducted a systematic investigation of the Dy−H system theoretically and experimentally focusing on DyH_3. CSP methods were used to predict new structures of DyH_3 at high pressure up to 220 GPa. In experiments, the Dy−H system was studied in an excess hydrogen environment at pressures up to ∼100 GPa in laser-heated diamond anvil cells (DACs). The direct chemical reaction between elemental dysprosium and hydrogen was carried inside DACs, coupled with synchrotron XRD. Our experimental results show that dysprosium reacts with hydrogen to form the $Fm\bar{3}m$ DyH_3 phase, which remains stable up to ∼100 GPa and ∼2000 K. Further theoretical calculations were used to verify the dynamical stability of the cubic DyH_3 phase in the experimental pressure range. A detailed *ab initio* investigation of the structural stability and electronic structure of the new high-pressure phases predicted for DyH_3 are presented here. Our results on the phase stability and EOS parameters of the DyH_3 phase are compared with other previously reported REH_3 phases to provide us with a better understanding of the thermodynamic and physical behavior of RE−H systems at high pressures.

■ EXPERIMENTAL DETAILS

High $P-T$ XRD experiments on the Dy−H system were carried out using laser-heated DACs. Pairs of beveled diamond anvils with 75−300 μm culets were used to reach the desired pressures. Rhenium gaskets were used to preindent from the initial thickness of 250 μm to ∼18 μm. Subsequently, a hole of ∼45 μm was drilled and served as a sample chamber. Dysprosium samples were prepared in a glovebox filled with argon, where both H_2O and O_2 concentrations were maintained below 0.1 ppm. The polycrystalline dysprosium sample was slightly pressed to ∼5 μm in thickness and 10 × 10 μm in size and then loaded into the sample chamber. High-purity hydrogen gas was loaded into the sample chamber using a high-pressure gas compressor by pumping hydrogen gas to ∼1.7 kilobar pressure at the Center for High Pressure Science & Technology Advanced Research (HPSTAR). Hydrogen served as a starting material as well as a hydrostatic medium. A tiny piece of gold (∼5 μm in diameter) was also placed next to the dysprosium sample and used as a pressure calibrant. Angle-dispersive XRD patterns were recorded on a

https://dx.doi.org/10.1021/acs.inorgchem.9b03078
Inorg. Chem. XXXX, XXX, XXX−XXX

PILATUS CdTe 1M detector at beamline 13-IDD of GeoSoilEnviroCARS (GSECARS) at the Advanced Photon Source (APS) of Argonne National Laboratory, USA. An incident X-ray with a wavelength of 0.3344 Å was focused onto a spot size of ~3 × 4 μm (fwhm) at the sample position, and a pinhole of 8 μm size was used as a cleanup slit, which helped in the collection on cleaner XRD patterns from the smallest area possible by cutting down the tails of the incident X-ray beam. An infrared pulsed laser with a wavelength of 1064 nm at beamline 13-IDD was focused onto the sample as a flat top of the laser heating spot size at around 10 μm in diameter for single-sided laser heating.[27] Several cycles of laser heating were carried out at each given pressure of 25, 40, 54, 68, 84, and 98 GPa, respectively. Laser pulses of a microsecond width at a rate of 10 kHz and accumulation of 200−300k frequency were used to heat the sample to 1000−2000 K. We intentionally limited laser heating to less than 2000 K to avoid a parasitic reaction with the Re gasket and to protect the diamonds from reacting with hydrogen under high $P-T$ conditions. *In situ* temperature measurements were carried out by fitting the slope of the measured thermal radiation spectra to a Planck radiation function.[28] The uncertainty in temperature measurements was typically less than ±100 K. The obtained raw images of XRD were integrated with DIOPTAS software.[29] Le Bail refinements were carried out using the FullProf and Jana programs.

■ COMPUTATIONAL DETAILS

We performed a systematic fixed-composition crystal structure search using the *ab initio* evolutionary algorithm USPEX,[30−32] which is capable of simultaneously searching for a stable structure with different numbers of formula units (fu) for a given composition. Here, we carried out crystal structure prediction calculations at 0, 50, 100, 150, 200 GPa for DyH_3 with up to 6 fu in the primitive cell. The first generation was produced randomly (using random symmetric[32] and topological[33] structure generators), while USPEX made subsequent generations with 20% random structures and 80% using heredity, soft mutation, and lattice mutation operators using the lowest enthalpy 60% of the population as parents. Structure relaxation was performed using the all-electron projector augmented wave (PAW) method[34] implemented in the VASP package[35] in the framework of DFT. Valence electron configurations $5p^6 5d^1 6s^2$ and $1s^1$ were used for dysprosium and hydrogen, respectively. The Perdew−Burke−Ernzerhof generalized gradient approximation (PBE-GGA) was used.[36] A plane-wave kinetic-energy cutoff of 1000 eV, hard PAW potentials, and dense Γ-centered k-point grids with reciprocal space resolution $2\pi \times 0.05$ Å^{-1} were employed to sample the Brillouin zone. To construct the phase diagram of DyH_3, the enthalpies were recalculated with increased precision at various pressures with a smaller pressure increment of 10 GPa. Electronic structure calculations for all of the predicted phases of DyH_3 were performed with the full-potential augmented-plane-wave + local orbital (APW +lo) approach as implemented in the Elk code.[37] The $5s^2 5p^6 4f^{10} 6s^2$ orbitals of Dy and $1s^1$ orbitals of H were treated as valence states. The exchange and correlation effects were treated with the PBE-GGA functional. The effect of the on-site Coulomb interaction among the $4f$ states of Dy was also considered within GGA+U (U = 6 eV).[38] The obtained electronic band structure and density of states with inclusion of the $4f$ states expectedly showed significant changes at the Fermi level for the predicted phases of DyH_3 within the studied pressure range.

■ RESULTS AND DISCUSSION

Synthesis of High-Pressure Phases in the Dy−H System in a DAC. Parts a and b of Figure 1 show the XRD patterns observed in our experiments in the compression and decompression cycles, respectively. After elemental Dy and H_2 were loaded in the sample chamber, an intermediate phase was observed at 9 GPa at ambient temperature (see Figure 1a). Similarly, the intermediate phase between hexagonal and cubic was also observed for other REH_3 compounds,[7,8,14,39−41] and

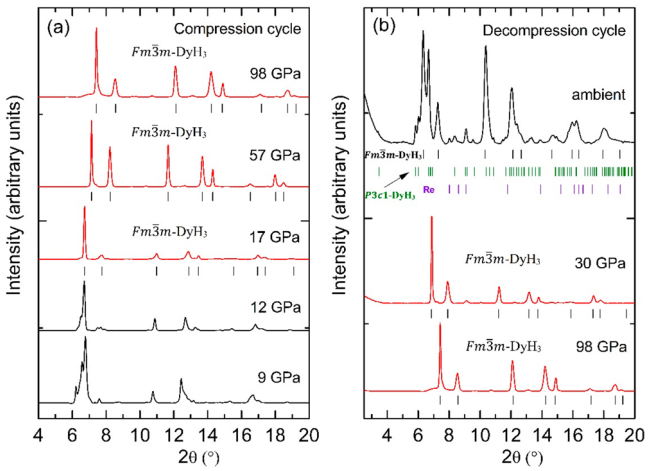

Figure 1. Representative integrated XRD patterns of the Dy−H system at high pressure and temperature. (a) In a compression cycle, a long-period polytype phase was observed at 9 GPa. Above 17 GPa, it transforms into $Fm\bar{3}m$ phase of DyH_3, which remains stable up to 98 GPa. (b) In a decompression cycle the $Fm\bar{3}m$ phase of DyH_3 was decompressed down to approximately 30 GPa. Under ambient conditions, the recovered sample was the $P\bar{3}c1$ phase of DyH_3 that coexisted with the $Fm\bar{3}m$ phase. The wavelength of the incident X-rays (λ) was 0.3344 Å.

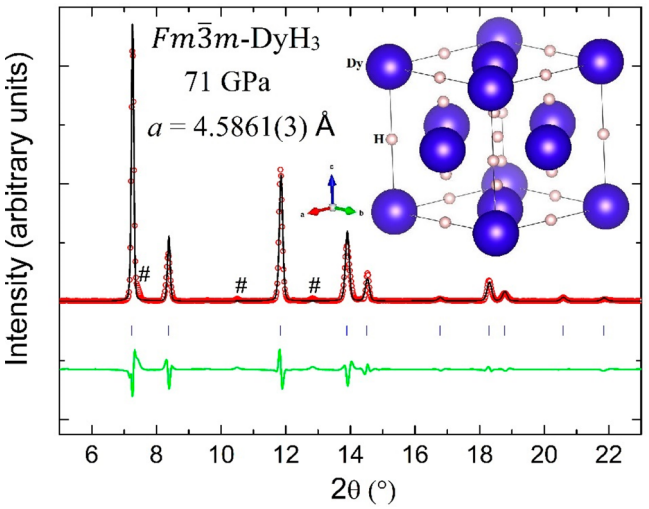

Figure 2. Refinement of the XRD pattern at 71 GPa. The inset shows crystal structure of the $Fm\bar{3}m$ phase of DyH_3 with hydrogen atoms midway between the Dy atoms. The black hash symbol denotes the unknown peaks.

in most cases, it was mixed with hexagonal and cubic phases. In the case of YH_3, the intermediate phase was observed with a long-period polytype structure.[8,42] In addition to an intermediate phase, the presence of bixbyite-type (i.e., fluorite-type with O vacancies) Dy_2O_3 was noticed in XRD patterns at 9 GPa, but on the basis of its XRD intensities it should minimally affect the experiments as a minor impurity phase. With further pressurization, a complete transformation into the $Fm\bar{3}m$ phase of DyH_3 was observed above 17 GPa. Previous high-pressure studies of DyH_3 also reported a sluggish hexagonal to cubic transition between 7 and 17 GPa.[16] The lattice parameter of the $Fm\bar{3}m$ phase of DyH_3 at 17 GPa is refined to be a = 4.9423(2) Å. Further, DyH_3 and H_2 were pressurized up to ~100 GPa and laser-heated up to 2000 K at

https://dx.doi.org/10.1021/acs.inorgchem.9b03078
Inorg. Chem. XXXX, XXX, XXX−XXX

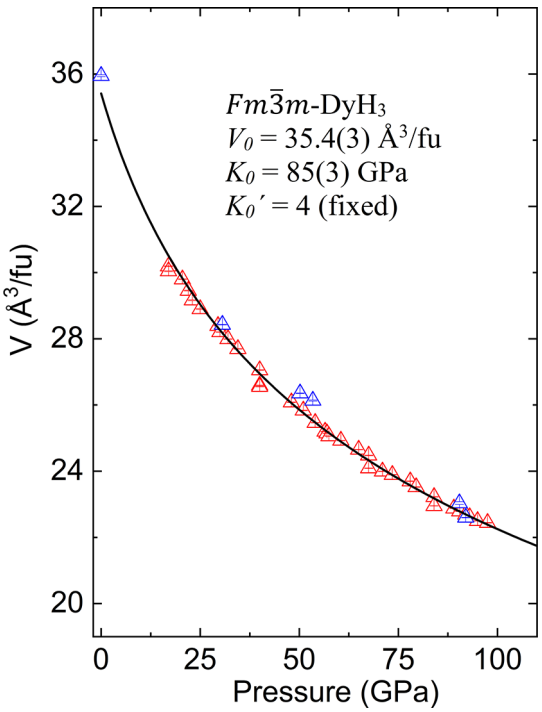

Figure 3. Unit cell volume of the $Fm\bar{3}m$ phase of DyH_3 as a function of pressure. The experimental volume per formula unit is plotted as a function of pressure. Red and blue open triangles represent the $Fm\bar{3}m$ phase of DyH_3 in the compression and decompression cycles, respectively. The black line represents the EOS fit.

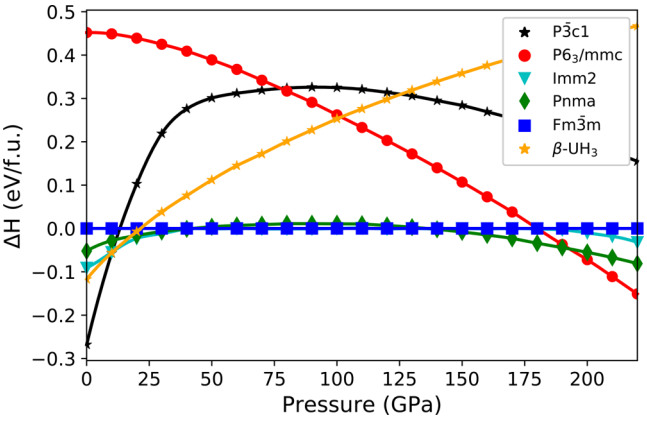

Figure 4. Calculated enthalpies of various predicted structures of DyH_3 as a function of pressure (relative to the cubic $Fm\bar{3}m$ phase). The $P\bar{3}c1$, *Imm*2, $Fm\bar{3}m$, *Pnma*, and $P6_3/mmc$ phases of DyH_3 became stable at 0, 11, 35, 135, and 194 GPa, respectively.

pressures of 25, 40, 54, 68, 84, and 98 GPa. Analysis of the XRD patterns for these $P-T$ conditions shows that the $Fm\bar{3}m$ phase of DyH_3 is the stable phase in the Dy−H system up to ∼100 GPa and ∼2000 K (Figure 1a). We did not observe the formation of any other phase with different stoichiometry or with a hydrogen content higher than that of the DyH_3 phase. The lattice parameter of the $Fm\bar{3}m$ phase of DyH_3 at 98 GPa is a = 4.4775(2) Å. Figure 2 shows the Le Bail refinement plot and crystal structure of DyH_3 at 71 GPa (R_p = 22.4%, R_{wp} = 28.3%). During the decompression cycle, the $Fm\bar{3}m$ phase of DyH_3 was present down to 30 GPa. With further decompression, the $P\bar{3}c1$ phase of DyH_3 emerged after complete decompression and coexisted with the $Fm\bar{3}m$ phase of DyH_3 at ambient pressure. The high-pressure $Fm\bar{3}m$ phase has also been recovered previously in studies on SmH_3 and DyH_3.[40] The lattice parameters of the $P\bar{3}c1$ phase of DyH_3 recovered at ambient pressure are a = 6.3849(8) Å and c = 6.596(1) Å and that for the $Fm\bar{3}m$ phase of DyH_3 is a = 5.239(1) Å. The EOS parameters of the $Fm\bar{3}m$ phase of DyH_3 obtained in the compression and decompression cycles are given in Figure 3. The unit cell volume of the $Fm\bar{3}m$ phase of DyH_3 as a function of pressure fitted using third-order Birch−Murnaghan EOS yielded the zero-pressure unit cell volume V_0 = 35.4(3) Å^3/fu and bulk modulus K_0 = 85(3) GPa, with fixed K_0' = 4.

Experiments did not observe the formation of β-UH_3 type or $P4/nmm$ phases of DyH_3 even after simultaneous compression and heating in excess hydrogen, as reported for the Ce−H and Pr−H systems.[13,24] In our calculations this structure is not stable, but becomes close to stability at pressures around 10 GPa.

Theoretical Prediction of Various DyH_3 Phases at High Pressures. First-principles calculations were performed to understand the chemistry of the Dy−H system at high pressure, along with the electronic structure, dynamical stability, and structural properties. Here, the focus was on the theoretical study of DyH_3, a compound that has been successfully synthesized. In previous theoretical studies, various compositions of the Dy−H system were predicted at high pressure, such as DyH, DyH_2, DyH_3, DyH_4, DyH_7, and Dy_5H_{14}.[11] Among the stable Dy−H phases predicted, only the DyH_3 phase was obtained in our experiment. Therefore, various fixed-composition calculations were performed at different pressures, to find the stable phases and clarify the phase diagram of DyH_3 as it undergoes a series of structural phase transitions within the studied pressure range of 0−220 GPa. In theoretical calculations, the $P\bar{3}c1$, *Imm*2, $Fm\bar{3}m$, *Pnma*, and $P6_3/mmc$ phases of DyH_3 were predicted to become stable at 0, 11, 35, 135, and 194 GPa, respectively (see the phase diagram in Figure 4).

Most REH_3 compounds crystallize in a hexagonal structure under ambient conditions with the possible space groups $P6_3$, $P6_3/mmc$, $P\bar{3}c1$, and $P6_3cm$.[9,43−50] Among them, the stable phase of DyH_3 crystallizes in a $P\bar{3}c1$ structure, similar to the other reported REH_3 phases such as (Er/Ho)H_3[43,45,47] and antiferromagnetic GdH_3.[46] Consistent with our predictions, the $P\bar{3}c1$ phase of DyH_3 was recovered under ambient conditions after complete decompression. Kong et al.[9] reported REH_3 (RE = Sm, Gd, Tb, Dy, Ho, Er, Tm, Lu) compounds that were stable in $P6_3cm$ symmetry under ambient conditions. Extensive studies have been devoted to understanding the structural transition sequences in REH_3 compounds. The known structural transition trends in this class of compounds are from an ambient $P6_3/mmc$ or $P\bar{3}c1$ structure to the $Fm\bar{3}m$ structure at high pressure. Kataoka et al.[48] were able to stabilize the high-pressure $Fm\bar{3}m$ phase under ambient conditions by doping it with an alkali or alkaline-earth metals (Li, K and Mg) for REH_3 (RE = Y, Gd, Dy). Interestingly, three new phases (*Imm*2, *Pnma*, and $P6_3/mmc$) of DyH_3 have been predicted in addition to the known phases ($P\bar{3}c1$, $Fm\bar{3}m$) in the studied pressure range of 0−220 GPa. The pressure-induced structural transition sequence in DyH_3 is as follows: $P\bar{3}c1 \rightarrow Imm2 \rightarrow Fm\bar{3}m \rightarrow Pnma \rightarrow P6_3/mmc$ at 11, 35, 135, and 194 GPa, respectively. The hexagonal to cubic transition is observed experimentally at 17 GPa and predicted the same transition at 35 GPa via an intermediate (*Imm*2)

https://dx.doi.org/10.1021/acs.inorgchem.9b03078
Inorg. Chem. XXXX, XXX, XXX−XXX

Table 1. Crystal Structures of the Predicted DyH_3 Phases[a]

phase	pressure range, GPa	volume, Å^3/fu	ρ, g/cm^3	lattice constants, Å	atom (Wyckoff site)	x	y	z
$P\bar{3}c1$	0−11	38.14	7.21	a = 6.328	Dy (6f)	0.6631	0	0.25
				b = 6.598	H_1 (12g)	0.6782	0.0289	−0.0921
					H_2 (2a)	0	0	0.25
					H_3 (4d)	0.3333	0.6667	0.8142
$Imm2$	11−35	29.67	9.26	a = 10.619	Dy_1 (2a)	0	0	0.4861
				b = 4.628	Dy_2 (4c)	0.6669	0	0.4230
				c = 3.621	H_1 (4c)	0.8334	0	0.8783
					H_2 (2b)	0	0.5	0.5502
					H_3 (8e)	0.8349	0.2542	0.4097
					H_4 (4d)	0	0.7479	0.0052
$Fm\bar{3}m$	35−135	26.62	10.33	a = 4.740	Dy (4a)	0	0	0
					H_1 (8c)	0.25	0.25	0.25
					H_2 (4b)	0.5	0.5	0.5
$Pnma$	135−194	20.25	13.57	a = 6.277	Dy (4c)	0.6353	0.25	0.8034
				b = 4.046	H_1 (4c)	0.8627	0.25	0.3163
				c = 3.189	H_2 (8d)	0.1077	0.4979	0.1863
$P6_3/mmc$	194−220	17.86	15.39	a = 2.773	Dy (2d)	0.3333	0.6667	0.75
				c = 5.360	H_1 (2a)	0	0	0
					H_2 (4f)	0.3333	0.6667	0.417

[a]Volumes, densities, lattice parameters, and atomic coordinates are given for different phases at the given pressures. Stability ranges are given for each phase.

Table 2. Theoretical Parameters of the Third-Order Birch−Murnaghan EOS[a]

structure	V_0, Å^3/fu	K_0, GPa	K_0'
$P\bar{3}c1$	38.1	80.7	4.05
	39.0[9]	79.8[9]	3.18[9]
$Imm2$	34.6	96.3	3.80
$Fm\bar{3}m$	34.2	96	3.69
	34.6	90.2	4 (fixed)
	35.4(3) exptl	85(3) exptl	4 (fixed) exptl
$Pnma$	34.5	97	3.75
$P6_3/mmc$	34.2	97	3.91

[a]Experimental data of this work are also added for the cubic phase.

phase, which is stable in the pressure range of 11−35 GPa. The $Pnma$ phase is also an energetically competitive for $Imm2$ and $Fm\bar{3}m$ phases. The $Imm2(Pnma) \rightarrow Fm\bar{3}m$ transition is a weakly first-order transition in nature, which is clearly seen from static enthalpy calculations in the pressure range of 20−35 GPa (see Figure 4). The predicted intermediate phases were not observed in our experiment at room temperature, which might be due to the anharmonic and quantum symmetrization effects.[51] Detailed structural information on the predicted phases is given in Table 1. Moreover, the intermediate ($C2/m$ and $Cmcm$) phases were also predicted for other REH_3 species such as ErH_3 and HoH_3 under high pressure.[43] The present study reveals the hidden intermediate phase ($Imm2$) for the investigated compound, DyH_3. The EOS parameter values of DyH_3 phases were calculated and fitted using a third-order Birch−Murnaghan EOS. The fitted parameters, such as the volume at zero pressure, bulk modulus, and first pressure derivative of bulk modulus for $Fm\bar{3}m$ DyH_3 are V_0 = 34.6 Å^3/fu and K_0 = 90.21 GPa with K_0' fixed at 4.

From our calculated phase diagram and EOS parameters, it is apparent that the cubic phase observed above 17 GPa with laser heating has DyH_3 stoichiometry. The experimental lattice parameter of the $Fm\bar{3}m$ phase at 30 GPa is a = 4.8319(1) Å (a = 4.812 Å theoretical). The theoretical EOS and fitted parameters in cubic DyH_3 are consistent with our experimental values (see Table 2). In the $Fm\bar{3}m$ phase of DyH_3, dysprosium atoms occupy the 4a (0,0,0) Wyckoff position and hydrogen atoms occupy the 8c (1/4,1/4,1/4) and 4b (1/2,1/2,1/2) Wyckoff positions. The theoretical third-order Birch−Murnaghan EOS fit to the $P-V$ data of DyH_3 along with experimental values are given in Table 2, which clearly shows $P\bar{3}c1$ has a lower bulk modulus of 80.7 GPa: i.e., higher compressibility in comparison with the high-pressure phase ($Fm\bar{3}m$ has a bulk modulus of 90.2 GPa) (see Table 2).

$P\bar{3}c1$-DyH_3 has a hexagonal fluocerite-type structure, with the nearest H−H distance of 2.10 Å and Dy−H distance of 2.13 Å at 0 GPa. In the $Fm\bar{3}m$ structure, the Dy−H bond distance is 2.12 Å at 20 GPa and 1.80 Å at 220 GPa. For DyH_3, theoretical calculations obtained a complex phase diagram with four phase transitions between 0 and 220 GPa. DyH_3 transforms to a cubic phase with space group $Fm\bar{3}m$ with 4 fu/cell at 35 GPa. $Fm\bar{3}m$ remains the most stable phase until 135 GPa and then transforms to a $Pnma$ phase. Finally, at pressures above 194 GPa, a hexagonal phase with 6 fu/cell becomes stable. Predicted stable phases of DyH_3 at different pressures are shown in Figure 5 (detailed structural information is provided in Table 1). A comparison of our results with the results obtained by Kong et al.[9] at ambient pressure shows consistency, in which the hexagonal fluocerite-type phase ($P\bar{3}c1$) has lattice parameters a = 6.328 Å and c = 6.598 Å (in comparison with the experimental values a = 6.3849(8) Å and c = 6.596(1) Å) recovered at ambient pressure.

Electronic Structure of DyH_3 Phases. Further, the electronic band structure and projected density of states (PDOS) were explored for the ambient- and high-pressure phases of DyH_3 with inclusion of $4f$ states for Dy as depicted in Figure 5. The inclusion of the $4f$ states for Dy along with Hubbard U (=6) parameter shows a significant change in the electronic properties at the Fermi level for all of the predicted phases of DyH_3 (see Figure 5). As illustrated in Figure 5, the predicted ambient- and high-pressure phases of DyH_3 show

https://dx.doi.org/10.1021/acs.inorgchem.9b03078
Inorg. Chem. XXXX, XXX, XXX−XXX

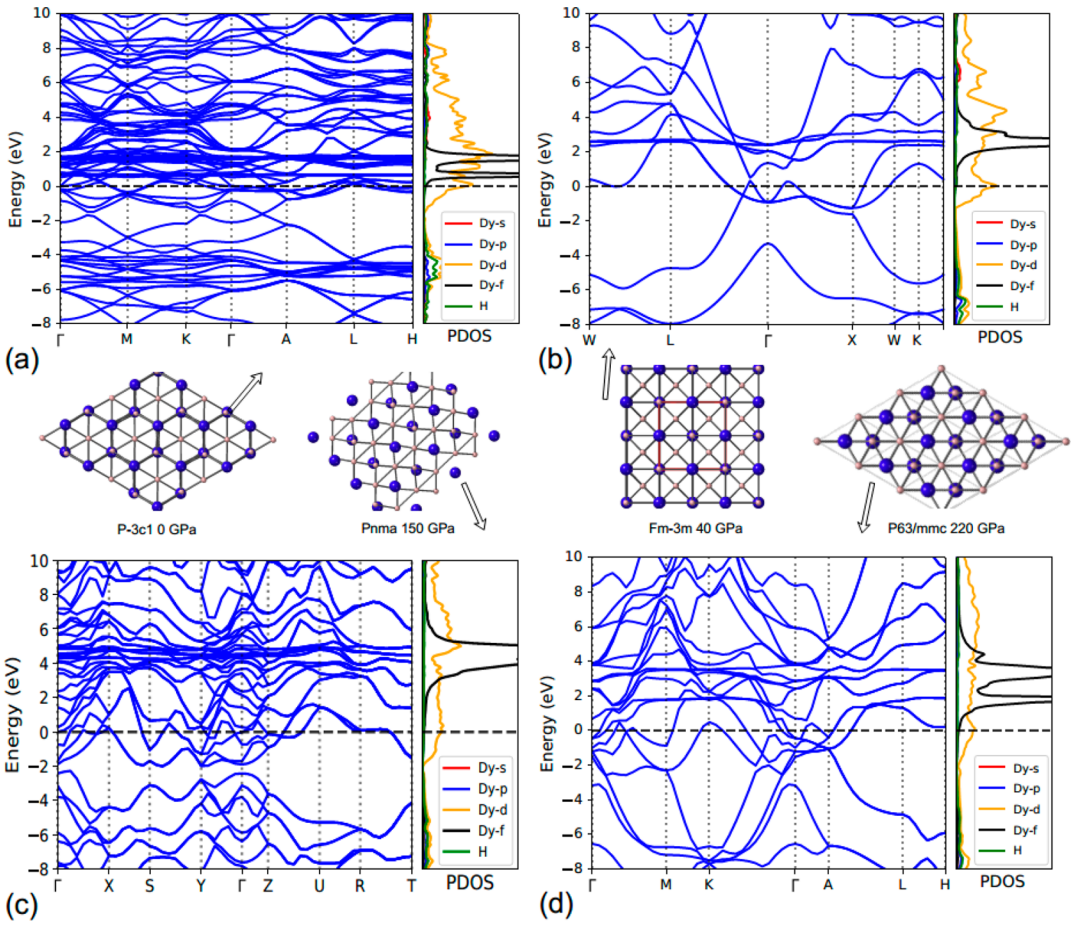

Figure 5. Electronic band structure and projected electronic density of states of (a) $P\bar{3}c1$, (b) $Fm\bar{3}m$, (c) *Pnma*, and (d) $P6_3/mmc$ DyH_3 at 0, 40, 150, and 220 GPa, respectively, including *4f* electrons using the GGA+*U* method (U = 6 eV).

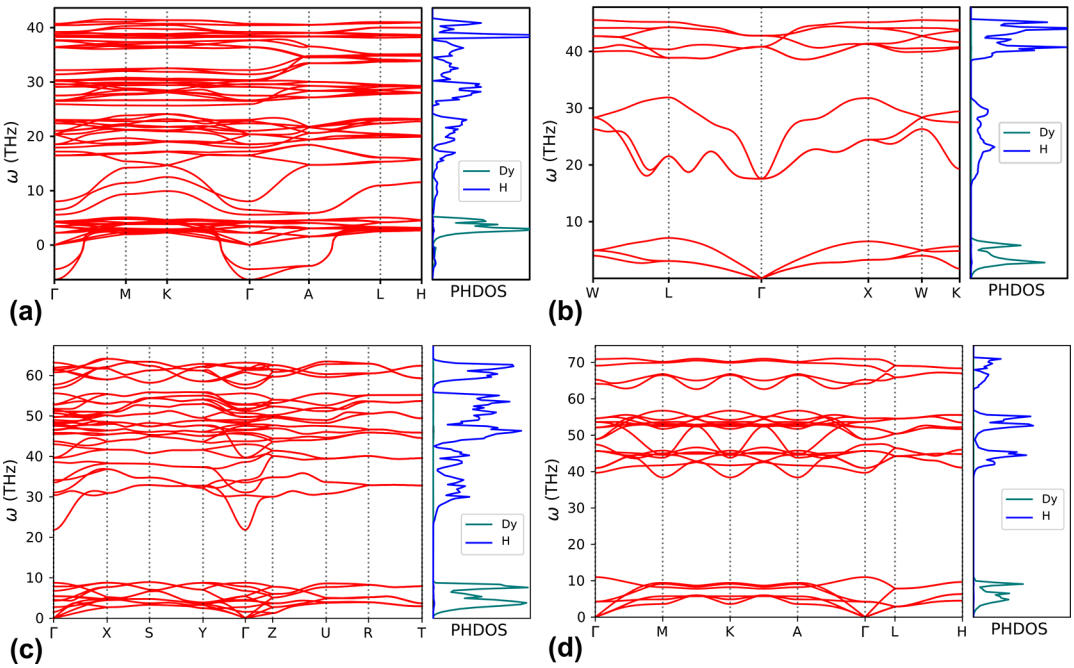

Figure 6. Calculated phonon dispersion curves and projected phonon density of states (PhDOS) of (a) $P\bar{3}c1$, (b) $Fm\bar{3}m$, (c) *Pnma*, and (d) $P6_3/mmc$ DyH_3 at 0, 40, 150, and 220 GPa, respectively, without inclusion of *4f* states.

metallic character, and the Fermi level is mainly dominated by Dy *d* states for all of the predicted phases.

Phonon Dispersion Curves of DyH_3 Phases. Phonon dispersion curves along with the projected phonon density of

https://dx.doi.org/10.1021/acs.inorgchem.9b03078
Inorg. Chem. XXXX, XXX, XXX−XXX

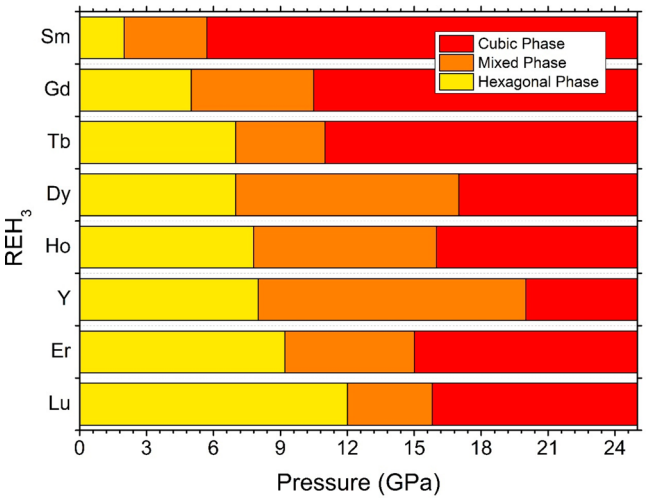

Figure 7. Phase diagram showing the ambient hexagonal $P6_3/mmc$ or $P\bar{3}c1$ phase, intermediate mixed phase region, and high-pressure cubic $Fm\bar{3}m$ phase region for REH_3 compounds. The REH_3 compound is denoted by the respective RE on the vertical axis. The yellow, orange, and red regions represent the pressure ranges for the hexagonal $P6_3/mmc$ or $P\bar{3}c1$ phase, mixed phase, and cubic $Fm\bar{3}m$ phase of REH_3, respectively.

states for the predicted ambient- and high-pressure phases of DyH_3 were calculated using a finite-displacement method as implemented in the PHONOPY code,[52] without inclusion of *4f* states. As shown in Figure 6, the absence of any imaginary frequencies in the whole Brillouin zone indicates dynamical stability of the predicted phases, except for the ambient phase, and anharmonic effects might play a role in stabilizing the ambient phase. As illustrated in the phonon density of states, the phonon bands are well separated due to the large difference in atomic mass between the Dy and H atoms (Figure 6). The low-frequency bands below 10 THz are mainly from the vibrations of Dy atoms, whereas modes between 20 and 70 THz are from the vibrations of H atoms.

Phase Transition Sequence and Systematics in REH_3 Compounds. In REH_3 systems, the high-pressure phase transition from ambient hexagonal $P6_3/mmc$ or $P\bar{3}c1$ phase to the cubic $Fm\bar{3}m$ phase through an intermediate mixed-phase region is a commonly observed sequence. Figure 7 shows the phase diagram of various REH_3 compounds, denoting the pressure range for the ambient hexagonal $P6_3/mmc$ or $P\bar{3}c1$ phase, intermediate mixed phase, and high-pressure cubic $Fm\bar{3}m$ phase region. RE elements and compounds bearing REs are known for their systematic trends in physical properties. Therefore, we plotted the phase transition pressure from the $P6_3/mmc$ or $P\bar{3}c1$ to $Fm\bar{3}m$ phase in REH_3 and the bulk modulus (K_0) of the high-pressure $Fm\bar{3}m$ phase of REH_3 with respect to the ionic radius[53] of the RE atom and with respect to the volume per formula unit (V/fu) of the ambient $P6_3/mmc$ or $P\bar{3}c1$ phase of REH_3 under ambient conditions, as shown in Figure 8. We can clearly see that the transition pressure decreases with the increasing ionic radius as well as with ambient V/fu of the $P6_3/mmc$ or $P\bar{3}c1$ phase. The reported bulk moduli of the high-pressure $Fm\bar{3}m$ phases of REH_3 were fitted with the Murnaghan EOS. For rational comparison, the reported V/fu data for the $Fm\bar{3}m$ phase of REH_3 compounds is fitted with the most frequently used third-order Birch−Murnaghan EOS with $K_0' = 4$ fixed. In Figure 8c,d, it can be seen that bulk modulus values for various REH_3 phases show a great deal of variation without any definite trend, which is probably due to the limited data range available for the previous studies. There is a huge difference in the bulk

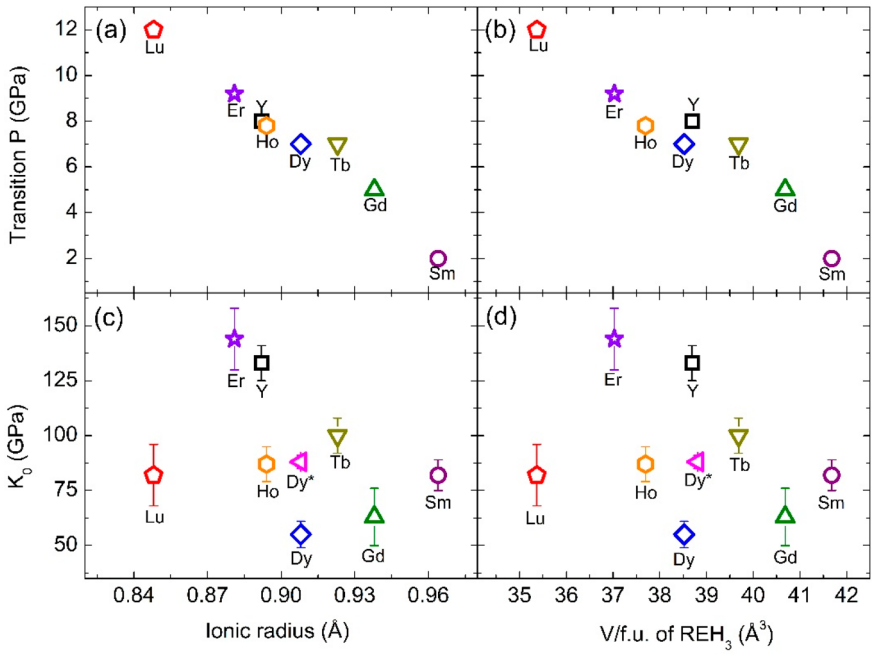

Figure 8. $P6_3/mmc$ or $P\bar{3}c1$ to $Fm\bar{3}m$ transition pressure and bulk modulus of the $Fm\bar{3}m$ phase of REH_3 plotted as a function of the ionic radius[53] of the RE atom in (a) and (c), respectively, and as a function of volume per formula unit of hexagonal REH_3 in (b) and (d), respectively. The bulk modulus was obtained by fitting the reported V/fu data of the $Fm\bar{3}m$ phases of REH_3 by a third-order Birch−Murnaghan EOS with fixed $K_0' = 4$. The name of the respective RE is mentioned in all the subfigures. (for references: YH_3,[8,14] SmH_3,[40] GdH_3,[39] TbH_3,[41] DyH_3,[16] DyH_3 (this study), HoH_3,[39] ErH_3,[7] LuH_3[39]).

https://dx.doi.org/10.1021/acs.inorgchem.9b03078
Inorg. Chem. XXXX, XXX, XXX−XXX

modulus of DyH_3 between the earlier study and present study. Previous studies on DyH_3 were only up to 31 GPa; hence, they could fit the pressure−volume data in the 17−31 GPa range with limited data points. The reported bulk modulus and its derivative fitted by the Murnaghan equation for DyH_3 are K_0 = 119 GPa and K_0' = 1.9, and if they are fitted with a third-order Birch−Murnaghan EOS, then the values are K_0 = 55(6) GPa and K_0' = 4 fixed. In comparison to a previous study,[16] we studied DyH_3 in a larger pressure range, perhaps the largest experimental range in comparison with any other REH_3 studied so far. Most of the reported trihydrides were studied below about 35 GPa. Thus, our EOS for DyH_3 is more reliable than the earlier reported EOS for the $Fm\bar{3}m$ phase of DyH_3. Most of the REH_3 phases studied in the past were with mineral oil as pressure-transmitting medium,[40] which likely can contaminate the sample. Hence, it is essential to revisit those studies with a better hydrostatic and inert medium in a higher pressure range.

■ SUMMARY

To summarize, experimental and theoretical studies were conducted to understand the Dy−H system, particularly the stability of DyH_3 under high pressures. Simultaneous compression and laser heating of elemental Dy with H_2 were performed inside a DAC to investigate the chemistry, $P-T$ stability, and EOS parameters of the Dy−H system. The $Fm\bar{3}m$ phase of DyH_3 was synthesized at 17 GPa and ambient temperature and remained stable up to at least 100 GPa and 2000 K. The *ab initio* CSP using the evolutionary USPEX method were used to explore the crystal structures, their stability, and electronic band structures to understand the structural transitions of DyH_3 at pressures up to 220 GPa. A series of structural transitions ($P\bar{3}c1 \rightarrow Imm2 \rightarrow Fm\bar{3}m \rightarrow Pnma \rightarrow P6_3/mmc$ at 11, 35, 135, and 194 GPa, respectively) were theoretically predicted in DyH_3. The calculated phonon dispersion curves reveal the dynamical stability of the predicted phases for DyH_3. The predicted intermediate phases in the static calculations might change to the cubic $Fm\bar{3}m$ phase when anharmonic and quantum symmetrization effects are considered. In REH_3 compounds, the ionic radii of the RE elements are found to be inversely proportional to the transition pressures from $P6_3/mmc$ (or $P\bar{3}c1$) to $Fm\bar{3}m$.

■ AUTHOR INFORMATION

Corresponding Authors

Jin Liu − *Center for High Pressure Science & Technology Advanced Research (HPSTAR), Beijing 100094, People's Republic of China;* orcid.org/0000-0002-1670-8199; Email: jin.liu@hpstar.ac.cn

Artem R. Oganov − *Department of Problems of Physics and Energetics, Moscow Institute of Physics and Technology, Dolgoprudny City 141700, Russia; Skolkovo Institute of Science and Technology, Skolkovo Innovation Center, Moscow 143026, Russia; International Center for Materials Discovery, Northwestern Polytechnical University, Xi'an 710072, People's Republic of China;* orcid.org/0000-0002-9315-1419; Email: a.oganov@skoltech.ru

Jung-Fu Lin − *Department of Geological Sciences, The University of Texas at Austin, Austin, Texas 78712, United States*; Email: afu@jsg.utexas.edu

Authors

Nilesh P. Salke − *Center for High Pressure Science & Technology Advanced Research (HPSTAR), Beijing 100094, People's Republic of China;* orcid.org/0000-0001-8662-9210

M. Mahdi Davari Esfahani − *Department of Geosciences, Center for Materials by Design and Institute for Advanced Computational Science, State University of New York, Stony Brook, New York 11794-2100, United States*

N. Yedukondalu − *Department of Geosciences, Center for Materials by Design and Institute for Advanced Computational Science, State University of New York, Stony Brook, New York 11794-2100, United States;* orcid.org/0000-0002-7650-7567

Youjun Zhang − *Institute of Atomic and Molecular Physics, Sichuan University, Chengdu 610065, People's Republic of China*

Ivan A. Kruglov − *Department of Problems of Physics and Energetics, Moscow Institute of Physics and Technology, Dolgoprudny City 141700, Russia; Dukhov Research Institute of Automatics (VNIIA), Moscow 127055, Russia*

Jianshi Zhou − *Department of Mechanical Engineering, The University of Texas at Austin, Austin, Texas 78712, United States;* orcid.org/0000-0002-7667-5640

Eran Greenberg − *Center for Advanced Radiation Sources, University of Chicago, Chicago, Illinois 60637, United States*

Vitali B. Prakapenka − *Center for Advanced Radiation Sources, University of Chicago, Chicago, Illinois 60637, United States*

Complete contact information is available at: https://pubs.acs.org/10.1021/acs.inorgchem.9b03078

Notes

The authors declare no competing financial interest.

■ ACKNOWLEDGMENTS

N.P.S. thanks HPSTAR for support. M.M.D.E. and N.Y. thank the National Science Foundation (EAR-1723160) for supporting this work. N.Y. thanks SERB/IUSSTF for providing financial support through a SERB Indo-US postdoctoral fellowship. J.Z. and J.-F.L. acknowledge support by the US Army (grant W911NF-16-1-0559). J.L. acknowledges support by the National Natural Science Foundation of China (U1930401). Y.Z. acknowledges support by the National Natural Science Foundation of China (No. 11872077) and the Fundamental Research Funds for the central universities (No. YJ201809). Portions of this work were performed at GeoSoilEnviroCARS (The University of Chicago, Sector 13), Advanced Photon Source (APS), Argonne National Laboratory. GeoSoilEnviroCARS is supported by the National Science Foundation-Earth Sciences (EAR-1634415) and Department of Energy-GeoSciences (DE-FG02-94ER14466). This research used resources of the Advanced Photon Source, a U.S. Department of Energy (DOE) Office of Science User Facility operated for the DOE Office of Science by Argonne National Laboratory under Contract No. DE-AC02-06CH11357.

■ REFERENCES

(1) Huiberts, J. N.; Griessen, R.; Rector, J. H.; Wijngaarden, R. J.; Dekker, J. P.; de Groot, D. G.; Koeman, N. J. Yttrium and lanthanum hydride films with switchable optical properties. *Nature* **1996**, *380*, 231.

(2) Ren, J.; Musyoka, N. M.; Langmi, H. W.; Mathe, M.; Liao, S. Current research trends and perspectives on materials-based hydrogen storage solutions: A critical review. *Int. J. Hydrogen Energy* **2017**, *42* (1), 289−311.
(3) Gor'kov, L. P.; Kresin, V. Z. Colloquium: High pressure and road to room temperature superconductivity. *Rev. Mod. Phys.* **2018**, *90* (1), No. 011001.
(4) Fukai, Y. *The Metal-Hydrogen System*; Springer: Berlin, Heidelberg, 2005; Vol. *21*.
(5) Strange, P.; Svane, A.; Temmerman, W. M.; Szotek, Z.; Winter, H. Understanding the valency of rare earths from first-principles theory. *Nature* **1999**, *399* (6738), 756−758.
(6) Janotti, A.; Van de Walle, C. G. Hydrogen multicentre bonds. *Nat. Mater.* **2007**, *6*, 44.
(7) Palasyuk, T.; Tkacz, M.; Vajda, P. High pressure studies of the erbium−hydrogen system. *Solid State Commun.* **2005**, *135* (4), 226−231.
(8) Machida, A.; Ohmura, A.; Watanuki, T.; Ikeda, T.; Aoki, K.; Nakano, S.; Takemura, K. X-ray diffraction investigation of the hexagonal−fcc structural transition in yttrium trihydride under hydrostatic pressure. *Solid State Commun.* **2006**, *138* (9), 436−440.
(9) Kong, B.; Zhang, L.; Chen, X.-R.; Zeng, T.-X.; Cai, L.-C. Structural relative stabilities and pressure-induced phase transitions for lanthanide trihydrides REH_3 (RE = Sm, Gd, Tb, Dy, Ho, Er, Tm, and Lu). *Phys. B* **2012**, *407* (12), 2050−2057.
(10) Peng, F.; Sun, Y.; Pickard, C. J.; Needs, R. J.; Wu, Q.; Ma, Y. Hydrogen Clathrate Structures in Rare Earth Hydrides at High Pressures: Possible Route to Room-Temperature Superconductivity. *Phys. Rev. Lett.* **2017**, *119* (10), 107001.
(11) Semenok, D. V.; Kruglov, I. A.; Savkin, I. A.; Kvashnin, A. G.; Oganov, A. R. On Distribution of Superconductivity in Metal Hydrides. *Curr. Opin. Solid State & Mater. Sci.* **2020**, in press.
(12) Geballe, Z. M.; Liu, H.; Mishra, A. K.; Ahart, M.; Somayazulu, M.; Meng, Y.; Baldini, M.; Hemley, R. J. Synthesis and Stability of Lanthanum Superhydrides. *Angew. Chem., Int. Ed.* **2018**, *57* (3), 688−692.
(13) Salke, N. P.; Davari Esfahani, M. M.; Zhang, Y.; Kruglov, I. A.; Zhou, J.; Wang, Y.; Greenberg, E.; Prakapenka, V. B.; Liu, J.; Oganov, A. R.; Lin, J.-F. Synthesis of clathrate cerium superhydride CeH_9 at 80−100 GPa with atomic hydrogen sublattice. *Nat. Commun.* **2019**, *10* (1), 4453.
(14) Palasyuk, T.; Tkacz, M. Hexagonal to cubic phase transition in YH_3 under high pressure. *Solid State Commun.* **2005**, *133* (7), 477−480.
(15) Tkacz, M.; Palasyuk, T. Pressure induced phase transformation of REH_3. *J. Alloys Compd.* **2007**, *446−447*, 593−597.
(16) Meng, H.; Palasyuk, T.; Drozd, V.; Tkacz, M. Study of phase stability and isotope effect in dysprosium trihydride at high pressure. *J. Alloys Compd.* **2017**, *722*, 946−952.
(17) Li, Y.; Hao, J.; Liu, H.; Tse, J. S.; Wang, Y.; Ma, Y. Pressure-stabilized superconductive yttrium hydrides. *Sci. Rep.* **2015**, *5*, 9948.
(18) Drozdov, A. P.; Kong, P. P.; Minkov, V. S.; Besedin, S. P.; Kuzovnikov, M. A.; Mozaffari, S.; Balicas, L.; Balakirev, F. F.; Graf, D. E.; Prakapenka, V. B.; Greenberg, E.; Knyazev, D. A.; Tkacz, M.; Eremets, M. I. Superconductivity at 250 K in lanthanum hydride under high pressures. *Nature* **2019**, *569* (7757), 528−531.
(19) Kong, P. P.; Minkov, V. S.; Kuzovnikov, M. A.; Besedin, S. P.; Drozdov, A. P.; Mozaffari, S.; Balicas, L.; Balakirev, F. F.; Prakapenka, V. B.; Greenberg, E.; Knyazev, D. A.; Eremets, M. I., Superconductivity up to 243 K in yttrium hydrides under high pressure. *arXiv* **2019**, *arXiv:1909.10482*.
(20) Liu, H.; Naumov, I. I.; Hoffmann, R.; Ashcroft, N. W.; Hemley, R. J. Potential high-T_c superconducting lanthanum and yttrium hydrides at high pressure. *Proc. Natl. Acad. Sci. U. S. A.* **2017**, *114* (27), 6990−6995.
(21) Duan, D.; Liu, Y.; Tian, F.; Li, D.; Huang, X.; Zhao, Z.; Yu, H.; Liu, B.; Tian, W.; Cui, T. Pressure-induced metallization of dense $(H_2S)_2H_2$ with high-Tc superconductivity. *Sci. Rep.* **2015**, *4*, 6968.
(22) Drozdov, A. P.; Eremets, M. I.; Troyan, I. A.; Ksenofontov, V.; Shylin, S. I. Conventional superconductivity at 203 K at high pressures in the sulfur hydride system. *Nature* **2015**, *525*, 73.
(23) Troyan, I. A.; Semenok, D. V.; Kvashnin, A. G.; Ivanova, A. G.; Prakapenka, V. B.; Greenberg, E.; Gavriliuk, A. G.; Lyubutin, I. S.; Struzhkin, V. V.; Oganov, A. R., Synthesis and Superconductivity of Yttrium Hexahydride Im-3m-YH_6. *arxiv* **2019**, *arXiv:1902.10206*.
(24) Zhou, D.; Semenok, D. V.; Duan, D.; Xie, H.; Huang, X.; Chen, W.; Li, X.; Liu, B.; Oganov, A. R.; Cui, T., Superconducting Praseodymium Superhydrides. *arXiv* **2019**, *arXiv:1904.06643*.
(25) Kim, D. Y.; Scheicher, R. H.; Ahuja, R. Predicted High-Temperature Superconducting State in the Hydrogen-Dense Transition-Metal Hydride YH_3 at 40 K and 17.7 GPa. *Phys. Rev. Lett.* **2009**, *103* (7), No. 077002.
(26) Friedt, J. M.; Shenoy, G. K.; Dunlap, B. D.; Westlake, D. G.; Aldred, A. T. Magnetic and crystal-field properties of dysprosium dihydrides and trihydrides from Mössbauer studies. *Phys. Rev. B: Condens. Matter Mater. Phys.* **1979**, *20* (1), 251−256.
(27) Prakapenka, V. B.; Kubo, A.; Kuznetsov, A.; Laskin, A.; Shkurikhin, O.; Dera, P.; Rivers, M. L.; Sutton, S. R. Advanced flat top laser heating system for high pressure research at GSECARS: application to the melting behavior of germanium. *High Pressure Res.* **2008**, *28* (3), 225−235.
(28) Shen, G.; Rivers, M. L.; Wang, Y.; Sutton, S. R. Laser heated diamond cell system at the Advanced Photon Source for in situ x-ray measurements at high pressure and temperature. *Rev. Sci. Instrum.* **2001**, *72* (2), 1273−1282.
(29) Prescher, C.; Prakapenka, V. B. DIOPTAS: a program for reduction of two-dimensional X-ray diffraction data and data exploration. *High Pressure Res.* **2015**, *35* (3), 223−230.
(30) Oganov, A. R.; Lyakhov, A. O.; Valle, M. How Evolutionary Crystal Structure Prediction Works—and Why. *Acc. Chem. Res.* **2011**, *44* (3), 227−237.
(31) Oganov, A. R.; Glass, C. W. Crystal structure prediction using ab initio evolutionary techniques: Principles and applications. *J. Chem. Phys.* **2006**, *124* (24), 244704.
(32) Lyakhov, A. O.; Oganov, A. R.; Stokes, H. T.; Zhu, Q. New developments in evolutionary structure prediction algorithm USPEX. *Comput. Phys. Commun.* **2013**, *184* (4), 1172−1182.
(33) Bushlanov, P. V.; Blatov, V. A.; Oganov, A. R. Topology-based crystal structure generator. *Comput. Phys. Commun.* **2019**, *236*, 1−7.
(34) Kresse, G.; Joubert, D. From ultrasoft pseudopotentials to the projector augmented-wave method. *Phys. Rev. B: Condens. Matter Mater. Phys.* **1999**, *59* (3), 1758−1775.
(35) Kresse, G.; Hafner, J. Ab initio molecular dynamics for liquid metals. *Phys. Rev. B: Condens. Matter Mater. Phys.* **1993**, *47* (1), 558−561.
(36) Perdew, J. P.; Burke, K.; Ernzerhof, M. Generalized Gradient Approximation Made Simple. *Phys. Rev. Lett.* **1996**, *77* (18), 3865−3868.
(37) *Computer code Elk, ver. 5.2.14*; http://elk.sourceforge.net.
(38) Warner, B.; El Hallak, F.; Atodiresei, N.; Seibt, P.; Prüser, H.; Caciuc, V.; Waters, M.; Fisher, A. J.; Blügel, S.; van Slageren, J.; Hirjibehedin, C. F. Sub-molecular modulation of a 4f driven Kondo resonance by surface-induced asymmetry. *Nat. Commun.* **2016**, *7* (1), 12785.
(39) Palasyuk, T.; Tkacz, M. Pressure-induced structural phase transition in rare-earth trihydrides. Part I. (GdH_3, HoH_3, LuH_3). *Solid State Commun.* **2005**, *133* (7), 481−486.
(40) Palasyuk, T.; Tkacz, M. Pressure-induced structural phase transition in rare-earth trihydrides. Part II. SmH_3 and compressibility systematics. *Solid State Commun.* **2007**, *141* (5), 302−305.
(41) Palasyuk, T.; Saxena, S.; Zaleski-Ejgierd, P.; Tkacz, M. High pressure studies of terbium trihydride. X-ray, Raman and DFT investigations. *J. Alloys Compd.* **2014**, *597*, 58−62.
(42) Machida, A.; Ohmura, A.; Watanuki, T.; Aoki, K.; Takemura, K. Long-period stacking structures in yttrium trihydride at high pressure. *Phys. Rev. B: Condens. Matter Mater. Phys.* **2007**, *76* (5), No. 052101.

https://dx.doi.org/10.1021/acs.inorgchem.9b03078
Inorg. Chem. XXXX, XXX, XXX−XXX

(43) Hou, P.; Tian, F.; Li, D.; Chu, B.; Zhao, Z.; Liu, B.; Cui, T. High-pressure phase transition of MH_3 (M: Er, Ho). *J. Chem. Phys.* **2014**, *141* (5), No. 054703.
(44) Antonov, V. E.; Bashkin, I. O.; Fedotov, V. K.; Khasanov, S. S.; Hansen, T.; Ivanov, A. S.; Kolesnikov, A. I.; Natkaniec, I. Crystal structure and lattice dynamics of high-pressure scandium trihydride. *Phys. Rev. B: Condens. Matter Mater. Phys.* **2006**, *73* (5), No. 054107.
(45) Kuzovnikov, M. A.; Eremets, M. I.; Drozdov, A. P.; Tkacz, M. Pressure-induced metallization in Erbium trihydride. *Solid State Commun.* **2017**, *263*, 23−26.
(46) Kong, B.; Xu, H.-B.; Wang, J.-R.; Wang, Y.-S.; Fu, Z.-J. The ground structure and the pressure-induced structural and electronic phase transitions for for rare-earth trihydride GdH_3. *J. Alloys Compd.* **2016**, *662*, 69−78.
(47) Moysés Araújo, C.; Ferreira da Silva, A.; Ahuja, R. Pressure-induced phase transition in ErH_3. *Phys. Status Solidi B* **2004**, *241* (14), 3219−3223.
(48) Kataoka, R.; Kimura, T.; Takeichi, N.; Kamegawa, A. Stabilization of Face-Centered Cubic High-Pressure Phase of REH_3 (RE = Y, Gd, Dy) at Ambient Pressure by Alkali or Alkaline-Earth Substitution. *Inorg. Chem.* **2018**, *57* (8), 4686−4692.
(49) Meng, H.; Kuzovnikov, M. A.; Tkacz, M. Phase stability of some rare earth trihydrides under high pressure. *Int. J. Hydrogen Energy* **2017**, *42* (49), 29344−29349.
(50) Zeng, T.-X.; Kong, B.; Diao, X.-F. First principles studies of the structural stability and lattice dynamics for rare earth hydridies REH_x (RE = Sm, Gd, Tb, Dy, Ho, Tm, x = 2, 3) under pressure. *J. Phys. Chem. Solids* **2019**, *126*, 196−208.
(51) Errea, I.; Calandra, M.; Pickard, C. J.; Nelson, J. R.; Needs, R. J.; Li, Y.; Liu, H.; Zhang, Y.; Ma, Y.; Mauri, F. Quantum hydrogen-bond symmetrization in the superconducting hydrogen sulfide system. *Nature* **2016**, *532*, 81.
(52) Togo, A.; Oba, F.; Tanaka, I. First-principles calculations of the ferroelastic transition between rutile-type and $CaCl_2$-type SiO_2 at high pressures. *Phys. Rev. B: Condens. Matter Mater. Phys.* **2008**, *78* (13), 134106.
(53) Shannon, R. D.; Prewitt, C. T. Effective ionic radii in oxides and fluorides. *Acta Crystallogr., Sect. B: Struct. Crystallogr. Cryst. Chem.* **1969**, *25* (5), 925−946.

https://dx.doi.org/10.1021/acs.inorgchem.9b03078
Inorg. Chem. XXXX, XXX, XXX−XXX